

Article

Effects of Aging under Stress on Mechanical Properties and Microstructure of EN AW 7075 Alloy

Seyed Vahid Sajadifar ^{1,*}, Philipp Krooß ¹, Hannes Fröck ², Benjamin Milkereit ^{2,3}, Olaf Kessler ^{2,3} and Thomas Niendorf ¹

- ¹ Institute of Materials Engineering, University of Kassel, Mönchebergstraße 3, 34125 Kassel, Germany; krooss@uni-kassel.de (P.K.); niendorf@uni-kassel.de (T.N.)
- ² Faculty of Mechanical Engineering and Marine Technology, University of Rostock, Albert-Einstein-Str. 2, 18059 Rostock, Germany; hannes.froeck@uni-rostock.de (H.F.); benjamin.milkereit@uni-rostock.de (B.M.); olaf.kessler@uni-rostock.de (O.K.)
- ³ Competence Centre CALOR, Department of Life, Light and Matter, University of Rostock, Albert-Einstein-Str. 25, 18059 Rostock, Germany
- * Correspondence: sajjadifar@uni-kassel.de; Tel.: +49-561-804-2949

Abstract: In the present study, microstructural and mechanical properties of EN AW 7075 following stress-aging were assessed. For this purpose, properties of stress-aged samples were compared with values obtained for conventionally aged counterparts. It is revealed that the strength and hardness of EN AW 7075 can be increased by the presence of external stresses during aging. Precipitation kinetics were found to be accelerated. The effects of conventional and stress-aging on the microstructure were analyzed using synergetic techniques: the differently aged samples were probed by differential scanning calorimetry (DSC) in order to characterize the precipitation processes. DSC was found to be an excellent screening tool for the analysis of precipitation processes during aging of this alloy with and without the presence of external stresses. Furthermore, using electron microscopy it was revealed that an improvement in mechanical properties can be correlated to changes in the morphologies and sizes of precipitates formed.

Keywords: high strength aluminum alloy; stress-aging; DSC; heat treatment; thermo-mechanical treatment



Citation: Sajadifar, S.V.; Krooß, P.; Fröck, H.; Milkereit, B.; Kessler, O.; Niendorf, T. Effects of Aging under Stress on Mechanical Properties and Microstructure of EN AW 7075 Alloy. *Metals* **2021**, *11*, 1142. <https://doi.org/10.3390/met11071142>

Academic Editors: Elisabetta Gariboldi and Sunghyuk Park

Received: 24 June 2021
Accepted: 15 July 2021
Published: 20 July 2021

Publisher's Note: MDPI stays neutral with regard to jurisdictional claims in published maps and institutional affiliations.



Copyright: © 2021 by the authors. Licensee MDPI, Basel, Switzerland. This article is an open access article distributed under the terms and conditions of the Creative Commons Attribution (CC BY) license (<https://creativecommons.org/licenses/by/4.0/>).

1. Introduction

Since many years, attempts have been made to substitute steels with alloys of low density to eventually reduce the weight of manufactured components. Among these so-called light alloys, high strength aluminum alloys were found to be outstanding candidates for this purpose [1–3]. Mechanical properties of high strength aluminum alloys can be tailored via heat treatment and thermo-mechanical processing [4–6]. Highest ultimate tensile strength (UTS) for common commercial high strength aluminum alloys was reported for EN AW 7075 alloy in T6 condition [6]. Generally, the UTS of EN AW 7075 alloy in T6 condition was found to be in the range of 490–580 MPa [7–9]. In combination to high strength, EN AW 7075-T6 has an acceptable formability being characterized by elongation at failure above 10% [8,9]. Thus, steels in many engineering applications could be generally replaced by high strength EN AW 7075 alloy, as this alloy features exceptional mechanical properties and, thus, can meet the demands needed for envisaged applications.

In recent years, efforts have been made to increase the strength of aluminum alloys by the employment of different thermo-mechanical processing routes. In these studies, the focus remained on precipitation hardening/aging since this heat treatment allows to establish parts with high strength and adequate ductility. Precipitation hardening not only improves the strength but also the fracture toughness of EN AW 7075 alloy [10]. The improvement in the fracture toughness of aged alloys can remarkably enhance crash resistance. Conventional aging treatments have been used for decades to modify mechanical properties of

aluminum alloys. Recently, aging under stress, termed creep aging or stress-aging, has drawn significant attention [11–16]. Stress-aging can be defined as precipitation hardening in the presence of external stress. The application of stress during aging strongly affects the precipitation kinetics [15]. Basically, stresses/strains during the aging treatment can result in a significant increase in nucleation sites for precipitates [11]. Further, volume changes due to precipitation interact with external stresses/strains [17]. Thus, the loading direction during stress-aging has an influence on the orientation and/or kinetics of the evolving precipitates [18]. Based on the results achieved in previous studies, it could be possible to change the orientation of precipitate plates by external stress and, thus, re-design the mechanical properties of manufactured parts. Thus, it is expected that this technique has an outstanding potential for many applications, e.g., in aerospace and automotive industries. Due to the unprecedented potential of stress-aging for increasing the material strength, this process was already employed for the production of complex stiffened aircraft panels made of EN AW 7475 [19].

Precipitation sequences during aging of a supersaturated solid solution (SSS) and important factors affecting the formation of different types of precipitates were already studied for EN AW 7075 and other alloys of the 7000 series [20–23]. The generalized precipitation sequence during aging treatment of this alloy is displayed in Figure 1. A heat treatment scheme with changes in aging time, aging temperature and cooling rate from the initial temperature level of solution heat treatment (SHT) is shown in Figure 1. Guinier–Preston (GP) zones and η' usually nucleate in the material at aging temperatures between 100 °C to 200 °C. At aging temperatures above 200 °C and increased aging times, respectively, η (MgZn_2) phase can be formed along the grain boundaries (GBs), subgrain boundaries or even in the grain interior, while higher temperatures and longer duration further promote coarsening of the precipitates [20]. Another important parameter in age hardening of this alloy is the cooling rate from SHT. It is well-documented that quenching this alloy in water (high cooling rate) typically results in the formation of the SSS [24]. However, a low cooling rate from SHT, less than about 30 K/s, can promote the formation of the coarse η precipitates even prior to aging [25]. Thus, aging temperature, duration and cooling rate from SHT are critical parameters in the precipitation process of aluminum alloys eventually allowing to directly design microstructure and final mechanical properties. However, the impact of external stresses during aging on the precipitation sequence of EN AW 7075 is not fully understood yet.

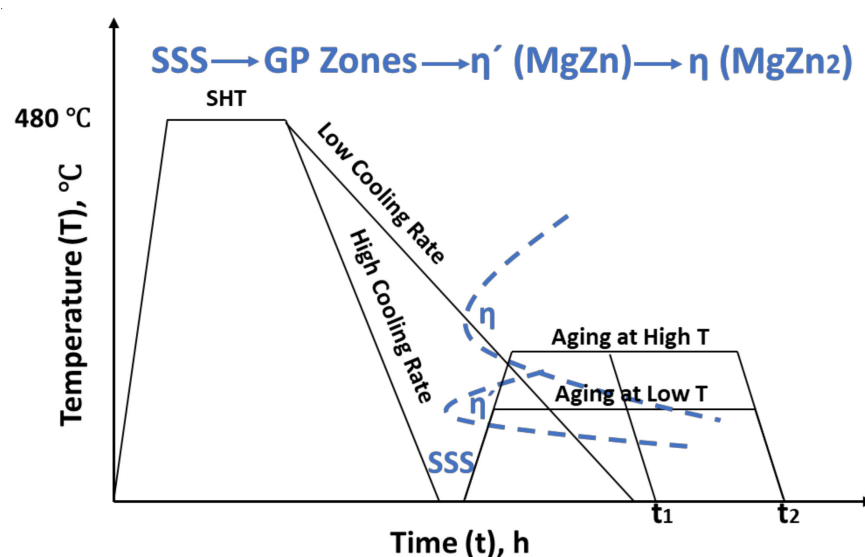


Figure 1. Precipitation sequence during artificial aging of EN AW 7075 alloy and schematic ranges related to nucleation of different precipitates with varying aging temperatures, durations and cooling rates from solution heat treatment (SHT) in EN AW 7075 alloy.

Differential scanning calorimetry (DSC) is a powerful method to characterize the solid phase transformation in-situ during heating as well as cooling of various materials, including aluminum alloys, over a wide temperature and scanning rate range [26]. During heating of age hardening aluminum alloys, various precipitates are formed and dissolved upon further heating to a level above their dissolution temperature. In general, dissolution reactions can be characterized as endothermic, while precipitation reactions proceed exothermic [27]. A few studies focused on DSC analysis of precipitates formed during stress-aging of aluminum alloys [28–31]. However, more comprehensive investigations of the impact of stress-aging on the microstructural evolution are crucially needed in order to gain a better understanding of the underlying mechanisms.

As detailed before, mechanical properties and resulting microstructure of stress-aged EN AW 7075 alloy are not yet well understood. Thus, the present investigation aims on establishing the correlation between details of thermo-mechanical processing, microstructural evolution and mechanical performance of stress-aged EN AW 7075. Hardness measurements and tensile testing were used to assess mechanical properties of both, conventionally and stress-aged counterparts. The microstructural evolution is captured by synergetic analytical techniques. Most importantly, thorough DSC analysis is used to characterize the precipitation kinetics in both, conventionally and stress aged EN AW 7075 samples. Finally, the obtained results provide pathways to realize superior components made of high strength aluminum alloys.

2. Materials and Methods

Extruded bars of EN AW 7075 in T6 condition with a diameter of 15 mm were received with the chemical composition as listed in Table 1. The chemical composition was determined via optical emission spectroscopy (OES) and is in accordance with the standard EN 573-3.

Table 1. Chemical composition of EN AW 7075 alloy determined by OES.

Element	Si	Fe	Cu	Mn	Mg	Cr	Zn	Ti	Zr	Al
EN AW 7075 (wt %)	0.10	0.11	1.49	0.03	2.38	0.20	5.57	0.03	0.04	Balance

Cylindrical dogbone shaped samples with dimensions highlighted in Figure 2a were machined from the as-received bars. Solution heat treatment was conducted in a roller hearth furnace at 480 °C for 30 min. SHT temperature and the soaking time were chosen based on previous studies [8,20,32–34]. After solution heat treatment, samples were quenched in water at a temperature of 20 °C. Afterwards, these samples were immediately mounted in the stress-aging rig to avoid natural aging. The stress-aging setup, including systems for controlled induction heating, as well as gas cooling and a process scheme are depicted in Figure 2c,d, respectively. Two aging temperatures of 105 °C and 120 °C, three aging times, i.e., 2 h, 15 h and 24 h, as well as a load free reference and two tensile stress values of 50 MPa and 200 MPa, were chosen to systematically address the impact of the process parameters in the stress-aging process on the final material properties. Stress values were selected in order to have different conditions namely, conventionally aged (0 MPa), stress-aged under low (50 MPa) and stress-aged under high (200 MPa) stresses. Whereas the lower stress level of 50 MPa is clearly below yield strength of 7075 T6 even at 200 °C, the higher stress level of 200 MPa approaches yield strength at 200 °C [35,36]. A thermocouple was attached to every sample by springs to measure temperature during experiments. The stress and elongation during stress-aging were determined using a conventional load cell and an extensometer, respectively.

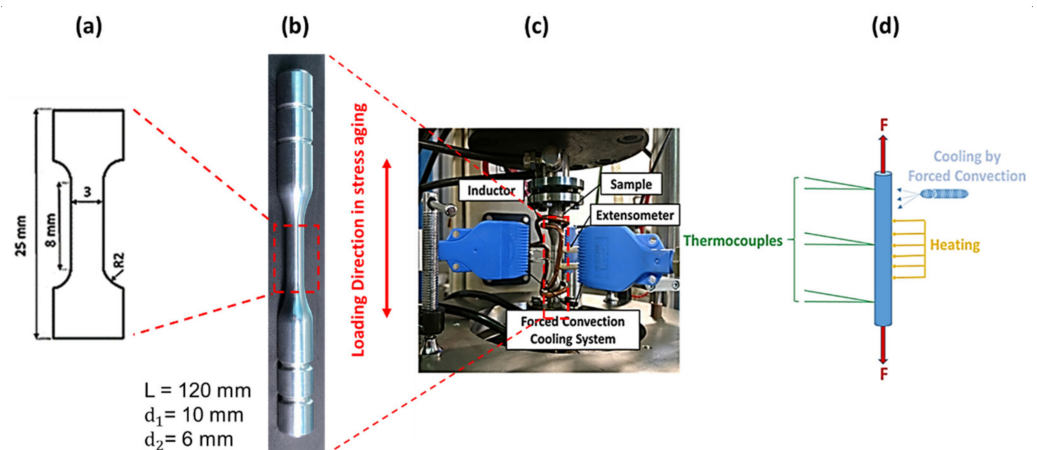


Figure 2. (a) Miniature flat samples cut from the initial gauge section for subsequent testing, (b) cylindrical dogbone samples used for stress-aging, (c) photograph showing the stress-aging setup and (d) schematic detailing the process.

Following the stress-aging process, miniature flat dogbone samples with a gauge length of 8 mm (Figure 2a) were electro-discharge machined (EDM) from the large samples (Figure 2b). The loading axis of the miniature sample was set parallel to the loading direction of the stress-aged sample as shown in Figure 2a. Before tensile testing, the miniature flat samples were ground to remove the EDM affected surface layers. Tensile experiments were carried out on the miniature samples at room temperature with a crosshead speed of 2 mm/min. Three tests were conducted for each condition and the average and scatter values are reported. An extensometer directly attached to the sample gauge length was used to measure the strain.

Vickers hardness tests were performed on the samples applying a force of 29.4 N (HV3) and 15 s indentation duration at room temperature. The reported hardness values for each condition are the average of 5 indents obtained from 5 various locations of the sample. Nanoindentation measurements were carried out using an Anton Paar NHT3 tester (Anton Paar GmbH, Graz, Austria). A Berkovich diamond indenter with a tip diameter of 100 nm was utilized. Maximum force, loading and unloading times were 10 mN and 30 s, respectively. Instrument approach and retract speeds were chosen as 2 µm/min. Nanoindentation experiments were conducted at room temperature.

DSC heating experiments were performed and evaluated as described in Reference [37]. The DSC measurements were performed using a Perkin-Elmer Pyris Diamond calorimeter equipped with a Huber TC 125W-MT cooler. Nitrogen gas was purged to provide a protective gas atmosphere. To prevent the measuring device from icing and to keep a constant ambient condition, the device was located under an acrylic glass box, this box being flushed with dry air. DSC measurements were performed on samples, which were composed of the remains of the cylindrical dogbone samples after cutting the miniature flat samples, i.e., semi-circular pieces, Figure 3. These pieces were loosely placed next to each other in a pure aluminum crucible and covered with a pure aluminum lid. The assembled samples had a mass of about 40 mg. Pure Al samples of similar mass were used as reference samples. Heating was applied from 30 °C to 490 °C at a constant rate of 1 K/s. At least two individual measurements and one baseline measurement were recorded for each condition. In the results section, the mean curve determined from the individual DSC measurements is shown.

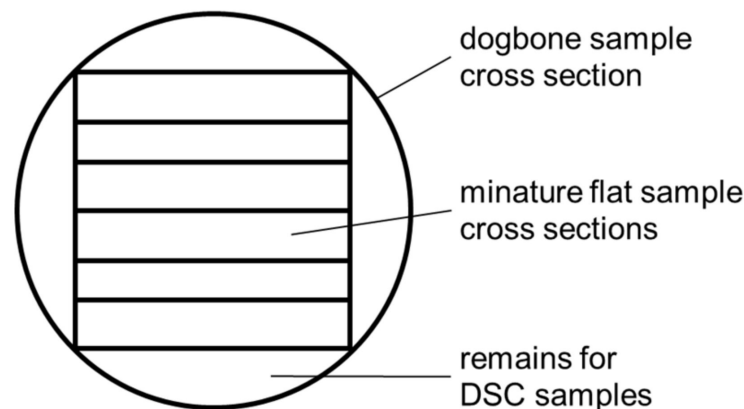


Figure 3. Differential scanning calorimetry (DSC) samples stemming from remains of the cylindrical dogbone samples after electro-discharge machining (EDM) cutting of the miniature flat samples.

Microstructural evolution was characterized using an optical microscope (OM) and a scanning electron microscope (SEM) (Zeiss ULTRA GEMINI, Jena, Germany) equipped with an electron backscatter diffraction (EBSD) unit operating at a nominal voltage of 20 kV. Both back-scattered electron (BSE) and secondary electron (SE) modes were employed to analyze the microstructure of the EN AW 7075 in various conditions. For microstructural studies, samples were first ground to 5 μm grit size and polished utilizing a colloidal silica suspension. Finally, these samples were further vibration-polished for 16 h using a colloidal silica solution with a particle size of 0.05 μm .

3. Results and Discussion

3.1. Mechanical Properties

The tensile properties of the as-received sample are summarized in Table 2. The EN AW 7075 alloy was received in T6 condition. UTS and elongation fulfill the standard EN 755-2, whereas YS is slightly below given values.

Table 2. Tensile properties of as-received material; standard deviations are reported in the table.

Material	YS (MPa)	UTS (MPa)	Elongation (%)
EN AW 7075 (T6)	447.4 \pm 3.5	577.3 \pm 2.7	11.2 \pm 0.9

+15]The mechanical properties of EN AW 7075 being stress-aged at 105 $^{\circ}\text{C}$ for various times under superposition of two external stress levels are shown in Figure 4. For comparison, samples were also aged for equal times without superimposed stress. As can be deduced from Figure 4, the external stress applied at 105 $^{\circ}\text{C}$ results in an accelerated aging as well as an improvement of strength almost without loss of ductility. It is worth noting that the highest strength and hardness values are obtained for the samples being stress-aged at 105 $^{\circ}\text{C}$ for 24 h at 200 MPa. Such an effect is thought to stem from the accelerated nucleation and growth of precipitates [38]. External stress/strain leads to the generation of dislocations and, hence, additional heterogeneous nucleation sites promoting precipitation [11,39].

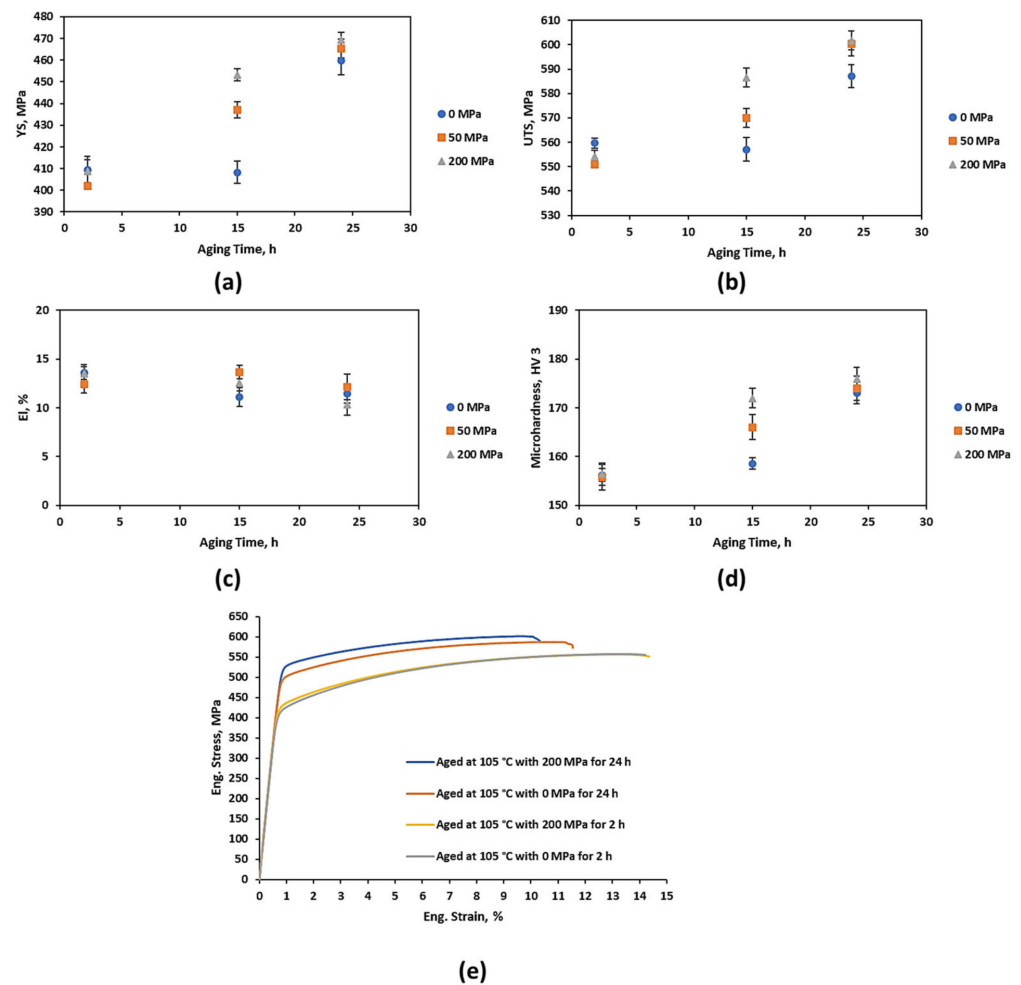


Figure 4. Mechanical properties of EN AW 7075 alloy aged at 105 °C with and without superimposed stress for various times: (a) yield strength, (b) ultimate tensile strength, (c) elongation at failure, (d) hardness; in (e) selected stress-strain curves are highlighted.

In order to gain a better understanding of the stress-aging process and to assess the effect of aging temperature, the EN AW 7075 samples were also aged at 120 °C. Except for the aging temperature, equal aging parameters i.e., aging times and external stresses were employed in order to allow for a meaningful comparison between both aging temperatures. Hardness and tensile properties of conventionally and stress-aged EN AW 7075, the latter being aged at 120 °C applying different aging times are depicted in Figure 5. Obviously, hardness, YS and UTS of both, conventionally and stress-aged samples, increase until reaching a peak at an aging time of 15 h. A variation of the aging duration in smaller steps may result in even higher maximum values. It must be noted that the strength and hardness values of the stress-aged samples are slightly higher than that of conventionally aged ones. This again can be attributed to the effect of external stress on the precipitation kinetics [15]. By comparing the evolution of mechanical properties for both aging temperatures, i.e., 105 °C and 120 °C, it becomes apparent that at 120 °C the precipitation kinetics are significantly increased, even in the load free aging condition (Figure 5). Furthermore, both conventionally and stress-aged conditions exhibit an over-aging at an aging temperature of 120 °C, applying an aging time of 24 h.

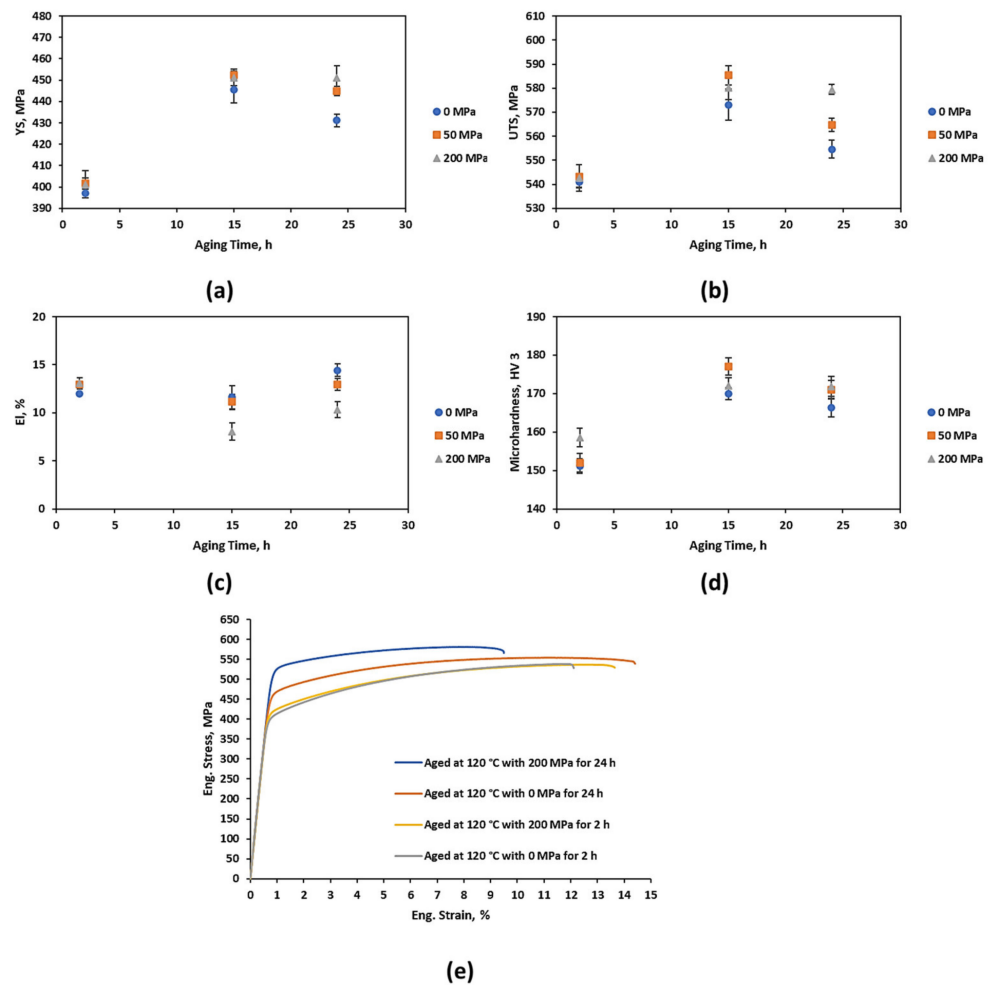


Figure 5. Mechanical properties of EN AW 7075 alloy aged at 120 °C with and without superimposed stress for various times: (a) yield strength, (b) ultimate tensile strength, (c) elongation at failure, (d) hardness; in (e) selected stress-strain curves are highlighted.

3.2. Microstructural Evolution

The microstructures of the as-received (T6), conventionally aged and stress-aged samples are shown in Figure 6. A bimodal microstructure composed of some equiaxed and recrystallized grains as well as columnar grains is seen (Figure 6a). Such a bimodal microstructure in the as-received condition can be linked to the initial hot extrusion process. Generally, inhomogeneous recrystallization during hot extrusion can lead to the formation of both, recrystallized regions consisting of fine grains and non-recrystallized regions with coarse columnar grains [40,41]. It is also worth noting that the texture of the non-recrystallized regions is near $\langle 101 \rangle$, whereas recrystallized regions are characterized by a random texture. The thermal treatments utilized in the present study had a small effect on the grain size distribution of the EN AW 7075 (Figure 6b,c). Microstructures of different conditions were examined by OM. Two exemplary micrographs are shown in Figure 6. Solution heat treatment and subsequent aging steps were already reported to have only minor influence on the overall grain sizes of EN AW 7075 [8,42,43]. In the present study, solution heat treatment parameters of all conditions were equal. During solution heat treatment of EN AW 7075, high-angle and low-angle grain boundaries as well as dislocations can be pinned based on the Zener pinning mechanism, at least prior to dissolution of precipitates [44,45]. Migration of low-angle boundaries and annihilation of point defects and dislocations are known to be the main mechanisms in case of recovery of aluminum alloys [46,47]. Motion of high-angle grain boundaries is reported to be the

main mechanism promoting recrystallization and subsequent grain growth [48,49]. As will be revealed in the remainder of the present work, based on DSC analysis, Zener pinning should not be effective during solution treatment as all precipitates are dissolved at this point. Thus, recovery diminished the driving force for recrystallization already in the as-received (T6) condition such that minimum changes in the grain sizes are seen here. Due to the high stacking-fault energy of Al alloys, a sufficient degree of recovery is expected [50].

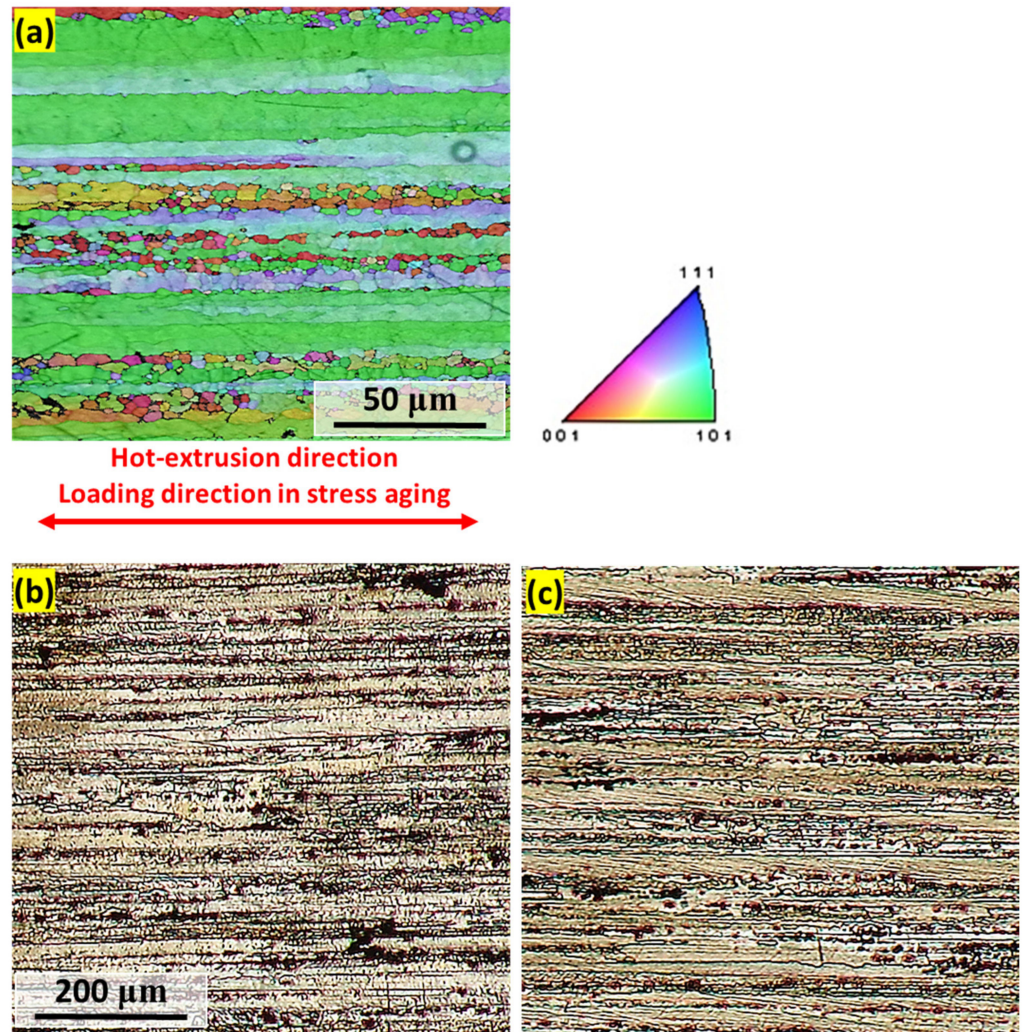


Figure 6. (a) EBSD inverse pole figure (IPF) map with superimposed image quality (IQ) of the as-received (T6) condition; optical micrograph of the samples aged at 120 °C (b) with 0 MPa for 2 h and (c) 50 MPa for 24 h. The optical micrographs were captured at the same magnification (see text for details).

For the visual assessment of coarse precipitates formed during the conventional and stress-aging procedures, BSE micrographs are shown in Figure 7. From this figure, it can be deduced that coarse precipitates along the grain boundaries (GBs) are formed in case of all conditions examined. Heterogeneous precipitation takes place at GBs since they are preferred nucleation sites [51,52]. It should also be pointed out that precipitates formed along the GBs coarsen with the increase of aging temperature and time, respectively. Higher aging temperature are known to significantly enhance solute diffusion along GBs [53]. Based on previous studies on EN AW 7075 alloys reported in literature [23,54–56], it can be expected that the coarse precipitates formed along the GBs are η -phase (Zn_2Mg).

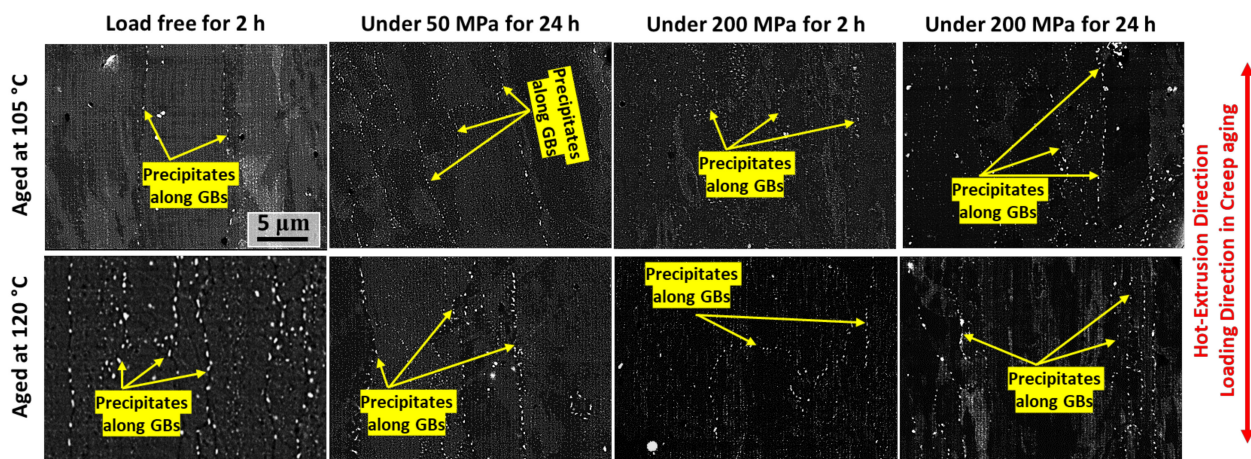


Figure 7. Back-scattered electron (BSE) contrast images of samples aged under different conditions. All images were captured at the same magnification (see text for details).

In order to assess the influence of GB precipitation in EN AW 7075, nanoindentation measurements were performed on the sample aged at 105 °C under 200 MPa for 15 h. To evaluate the localized effects of precipitate size and type on the mechanical properties, measurements were performed in the grain interior and along a grain boundary. The depth of penetration as a function of the applied load and location of the indent is shown in Figure 8. The results imply that the depth of penetration was slightly higher for the measurements conducted alongside the grain boundary, eventually indicating lower hardness and lower strength, respectively, of the material in the direct vicinity of GBs. As is known from literature, the formation of a precipitate free zone (PFZ) takes place, being rationalized by the migration of solute elements and the accompanying growth of precipitates alongside the GBs. Eventually, this kind of localized microstructure evolution consumes the alloying elements needed for precipitation from the surrounding volume. Such PFZs are known to promote low hardness in aluminum alloys on the local scale [57,58].

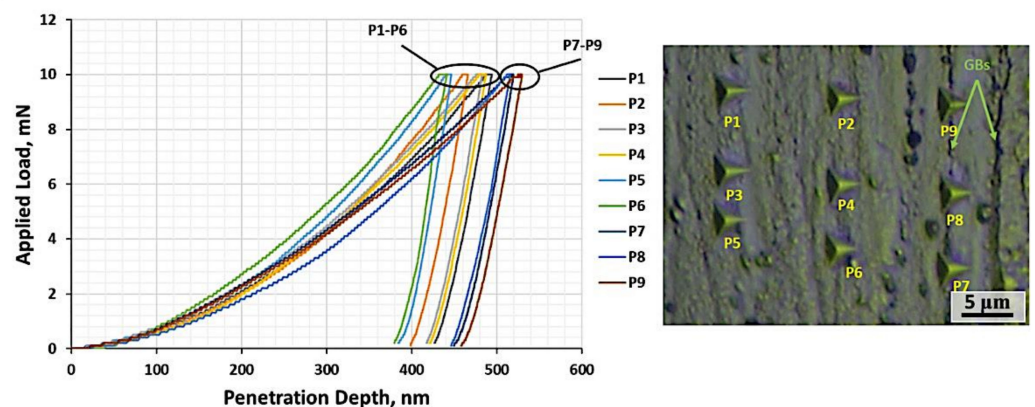


Figure 8. Nanoindentation measurements conducted focusing on the sample aged at 105 °C under 200 MPa for 15 h at various points (P). Locations of points are displayed on the right (see text for details).

3.3. DSC Measurements

The DSC heating curves (see Figure 9) show clear differences in the dissolution and precipitation behavior between stress-free and stress-aged samples. The peaks of the heating curve have been named in alphabetical order in accordance to Reference [27] for clarity to ease discussion. Dissolution Peaks are named in capital letters while precipitation Peaks are described in lower case letters. During the heating process, a first endothermic peak

(A) appears from approx. 100 °C being associated with the dissolution of GP-zones [59]. This first endothermic peak is very similar in peak value and shape for all heating curves of the different conditions. Subsequently, a large endothermic peak (B) is resolved from 170 to 250 °C, corresponding to the dissolution of η' [60]. During this dissolution reaction, the precipitates that have formed during the previous aging treatment are dissolved. Thus, on the basis of the appearance of this peak the precipitation process promoted by the initial stress-aging treatment conducted in present work can be assessed. It is important to mention that all heating curves were recorded with the same heating rate. Thus, any biasing effect induced by differences in dynamic suppression of individual reactions due to different heating rates can be excluded. Only based on such strict experimental boundary conditions individual peaks can be compared with each other [37].

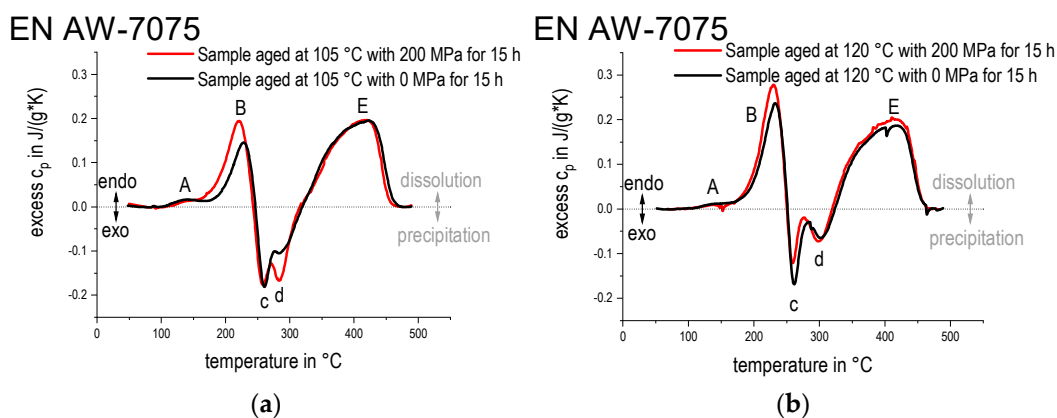


Figure 9. DSC heating experiments conducted using the samples aged at (a) 105 °C and (b) 120 °C for 15 h with and without superimposed stress of 200 MPa.

The results obtained for the two different aging temperatures can be directly compared with each other. It can be seen that the peak (B) in the heating curves is more pronounced after aging at 120 °C for 15 h than after aging at 105 °C for 15 h. Furthermore, it can be seen that (at each aging temperature) in case of the superposition of the tensile stress, the dissolution peak (B) in the heating curves is more pronounced than in the stressless case. Above 250 °C, the exothermic double peak (c + d) is seen in all heating curves. It is related to the precipitation of η from the solid solution after having dissolved η' as well as the direct transformation of $\eta' \rightarrow \eta$ [60]. Peak (c) is characterized by almost the same intensity and course for all examined conditions. Clear differences can still be seen in case of peak (d). The heating curves after aging at 120 °C are characterized by the same course for peak (d), while peak (d) is much more pronounced after stress-aging at 105 °C. The results obtained based on DSC analysis will be further discussed in the following chapter. The final endothermic peak (E) shows dissolution of η . This peak follows the same course for all conditions considered here.

3.4. Heat Treatment-Microstructure-Property Relationships

The DSC heating curves of the different conditions show clear differences in dissolution and precipitation behavior, i.e., in case of the (at different temperatures) stressless and stress-aged conditions (Figure 9). First, the impact of aging temperature is considered: Obviously, the endothermic peak (B) for dissolution of η' is more pronounced after aging at 120 °C for 15 h than after aging at 105 °C for 15 h (for both stressless and stress-aged conditions). From this observation, it can be concluded that a larger fraction of strengthening η' precipitates has been formed during aging at 120 °C during aging at 105 °C. This is confirmed by higher yield strength as well as higher hardness after aging at 120 °C for 15 h as compared to the condition obtained by aging at 105 °C for 15 h (compare Figures 4 and 5). It should also be noted that the increase in the strength of the alloy is not only linked to the volume fraction of introduced precipitates but also their morphology [23,61].

It was previously reported that precipitates with various morphologies can be introduced by different heat treatments and thermo-mechanical processing of EN AW 7075 alloy.

Obviously, the DSC heating curves not only are affected by the aging temperature but also by the superimposed tensile stress applied during the aging process. The first dissolution peak (B) is more pronounced in the heating curves of the stress-aged conditions compared to stressless aged conditions (for both aging temperatures, however, most pronounced after aging at 105 °C for 15 h). From this finding it can be concluded that the application of tensile stress is effective to promote precipitation processes and, eventually, a higher fraction of strengthening η' precipitates is formed during stress-aging. This is also confirmed by the higher yield strength found after stress-aging as compared to stressless aging (Figures 4a and 5a). Figure 10 details the correlation between yield strength and integrated dissolution heat of peaks (A) and (B), i.e., dissolution of GP and η' . Clearly, the yield strength increases with increasing dissolution heat, the latter thus being related to initial presence of these strengthening precipitates. In conclusion, DSC heating experiments can be systematically applied to survey the success of previous stress-aging procedures.

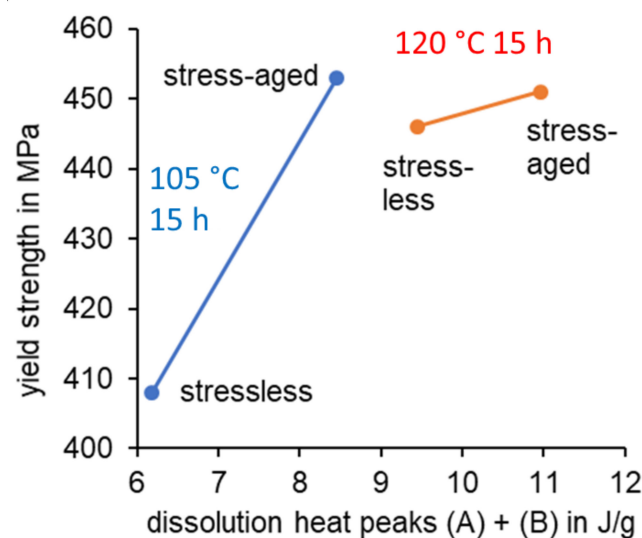


Figure 10. Correlation between yield strength and the summated dissolution heat of peaks (A) and (B), i.e., dissolution of GP and η' ; stressless and stress-aged samples were considered, superimposed stresses were 0 MPa and 200 MPa, respectively.

Due to the strong overlap of the exothermic peaks (c) and (d), both being related the precipitation of η , an in-depth interpretation of these peaks is difficult. It can be seen that the heating curves after aging at 120 °C for 15 h are characterized by a kind of similar appearance of peaks (c) and (d) regardless of the superimposed tensile stress applied during aging. However, the heating curves deviate significantly after aging at 105 °C for 15 h in the temperature range of 270 °C to 300 °C, see peak (d) in Figure 9a. This has to be investigated in more detail in future. It may be correlated with the precipitation of η from solid solution after having dissolved η' or the direct transformation from η' to η [60].

As elaborated earlier (Figures 4 and 5), the superposition of stress during aging considerably influences the precipitation kinetics [15]. Thus, as verified by DSC measurements (Figure 9), aging treatments with superimposed external stresses provide for a higher fraction of nucleation sites for precipitation in aluminum alloys [11,39]. In general, external stresses/strains and changes in volume induced by the phases evolving during precipitation affect microstructure and mechanical properties of the material [17]. A higher fraction of fine and dispersed precipitates in the stress-aged condition can be named as the main reason for the higher hardness as well as the superior YS and UTS values compared to those of the conventionally aged condition [19,62]. Previous studies already indicated that stress-aging causes the formation of a higher fraction of fine precipitates in aluminum

alloys (others than EN AW 7075) due to the generation of dislocations acting as nucleation sites [63–65]. Two different superimposed stress levels were applied during the aging treatment of the EN AW 7075 alloy in order to assess the impact of the absolute value of stress on the final microstructure and the mechanical properties. Even at a relatively low level of stress (50 MPa in the present study), the mechanical properties of this alloy are altered. It was previously reported that aging even under an elastic tensile load of only 25 MPa already promotes a more rapid formation of secondary phases in EN AW 7075 [66]. However, the present study aimed to explore a wider range of external stresses up to 200 MPa in order to establish profound heat treatment-microstructure-property relationships for this alloy. The existence of stress fields during aging is known to enhance the diffusion rates of the solute atoms, e.g., Zn, Mg and Cu, within the bulk promoted by vacancies. With the increase in the external stress value from 50 MPa to 200 MPa, further enhancement in terms of generation of dislocations is expected to take place additionally. Thus, faster precipitation kinetics were expected for the samples aged superimposed by such a high external stress level [11]. However, it should be noted that precipitation kinetics are only expected to be further accelerated up to a certain combination of temperature and stress. Especially at the relatively high aging temperature considered here, the precipitation kinetics already are very fast despite the additional employment of superimposed stress. In addition to the impact of superimposed external stresses on the sizes and morphologies of precipitates, stress-aging leads to the reduction of lateral dimensions of PFZs as reported in previous studies [18,67,68]. In these studies, all focusing on Al-Cu-Mg-Ag and Al-Cu alloys, high degrees of strain during stress-aging were employed resulting in the introduction of dislocations as preferential sites for the nucleation of second phases. Finally, this led to the formation of fine and disperse precipitates and, hence, reduction in the width of PFZs. Creep aging can further result in a preferential orientation of the precipitates. Although changes in the orientation of η precipitates due to the stress-aging were not evident in EN AW 7075 [15], an aligned precursor θ''/θ' precipitate structure has been found in an aluminum-copper alloy [18].

Mechanical properties and microstructural features obtained and discussed in the present study clearly reveal that DSC is a reliable screening tool for the evaluation of the effect of any kind of heat treatment including stress-aging in high-strength Al alloys. DSC analysis verified that the improvement in the mechanical properties of EN AW 7075 alloy enabled by the stress-aging can be linked to the formation of a higher fraction of strengthening η' precipitates.

4. Conclusions

The effect of artificial aging under superimposed external stresses on the mechanical properties and microstructure of EN AW 7075 alloy was explored in present work. The following conclusion can be drawn based on the results obtained:

- (i) Hardness and tensile tests revealed that stress-aging led to an enhanced peak strength of EN AW 7075 alloy. Aging under stress was capable of accelerating the kinetics of the precipitation process.
- (ii) The DSC measurements clearly show that the increase in the strength of stress-aged EN AW 7075 alloy can be rationalized based on both volume fraction and morphology of introduced precipitates. On the one hand, a higher volume fraction of strengthening η' precipitates has been formed during aging at 120 °C as compared to aging at 105 °C for the same duration. On the other hand, it is shown that an applied tensile stress of 200 MPa during aging leads to a higher fraction of strengthening η' precipitates as stressless aging. Dissolution heat of peaks being related to GP and η' precipitates is in good agreement to yield strength of all material conditions including those after stress-aging.
- (iii) In addition, DSC hints on an influence of stress-aging on the course of further η formation. This has to be investigated in more detail in the future.

- (iv) In summary, DSC proved to be a good screening tool for the assessment of the impact of any kind of heat treatment including stress aging in EN AW 7075 alloy.

Author Contributions: Conceptualization, S.V.S., P.K., H.F. and B.M.; Methodology, S.V.S., P.K., H.F. and B.M.; Validation, S.V.S., P.K., H.F., B.M., O.K. and T.N.; Investigation, S.V.S., P.K., H.F. and B.M.; Writing—Original Draft Preparation, S.V.S., P.K., H.F. and B.M.; Writing—Review & Editing, S.V.S., P.K., H.F., B.M., O.K. and T.N.; Visualization, S.V.S., P.K., H.F., B.M., O.K. and T.N.; Supervision, O.K. and T.N. All authors have read and agreed to the published version of the manuscript.

Funding: The authors would like to thank financial support from the Hessen State Ministry for Higher Education, Research and the Arts-Initiative for the Development of Scientific and Economic Excellence (LOEWE) for the project ALLEGRO (Subprojects B1).

Data Availability Statement: Not applicable.

Acknowledgments: The authors would also to thank Davoud Kouhi Anbaran for his assistance in conducting the stress-aging experiments.

Conflicts of Interest: The authors declare no conflict of interest.

References

1. Tisza, M.; Czinege, I. Comparative study of the application of steels and aluminium in lightweight production of automotive parts. *Int. J. Light. Mater. Manuf.* **2018**, *1*, 229–238. [[CrossRef](#)]
2. Liu, Y.; Zhu, Z.; Wang, Z.; Zhu, B.; Wang, Y.; Zhang, Y. Formability and lubrication of a B-pillar in hot stamping with 6061 and 7075 aluminum alloy sheets. *Procedia Eng.* **2017**, *207*, 723–728. [[CrossRef](#)]
3. Poznak, A.; Freiberg, D.; Sanders, P. Automotive Wrought Aluminium Alloys. *Fundam. Alum. Metall.* **2018**, 333–386. [[CrossRef](#)]
4. Starke, E.A.; Staley, J.T. Application of modern aluminum alloys to aircraft. *Prog. Aerosp. Sci.* **1996**, *32*, 131–172. [[CrossRef](#)]
5. Li, X.-M.; Starink, M.J. Effect of compositional variations on characteristics of coarse intermetallic particles in overaged 7000 aluminium alloys. *Mater. Sci. Technol.* **2001**, *17*, 1324–1328. [[CrossRef](#)]
6. Senthil, K.; Iqbal, M.A.; Chandel, P.S.; Gupta, N. Study of the constitutive behavior of 7075-T651 aluminum alloy. *Int. J. Impact Eng.* **2017**, *108*, 171–190. [[CrossRef](#)]
7. Hu, B.; Richardson, I.M. Microstructure and mechanical properties of AA7075(T6) hybrid laser/GMA welds. *Mater. Sci. Eng. A* **2007**, *459*, 94–100. [[CrossRef](#)]
8. Sajadifar, S.V.; Scharifi, E.; Weidig, U.; Steinhoff, K.; Niendorf, T. Effect of Tool Temperature on Mechanical Properties and Microstructure of Thermo-Mechanically Processed AA6082 and AA7075 Aluminum Alloys. *HTM J. Heat Treat. Mater.* **2020**, *75*, 177–191. [[CrossRef](#)]
9. Sajadifar, S.V.; Scharifi, E.; Weidig, U.; Steinhoff, K.; Niendorf, T. Performance of Thermo-Mechanically Processed AA7075 Alloy at Elevated Temperatures—From Microstructure to Mechanical Properties. *Metals* **2020**, *10*, 884. [[CrossRef](#)]
10. Das, P.; Jayaganthan, R.; Singh, I.V. Tensile and impact-toughness behaviour of cryorolled Al 7075 alloy. *Mater. Des.* **2011**, *32*, 1298–1305. [[CrossRef](#)]
11. Kolar, M.; Pedersen, K.O.; Gulbrandsen-Dahl, S.; Marthinsen, K. Combined effect of deformation and artificial aging on mechanical properties of Al-Mg-Si Alloy. *Trans. Nonferrous Met. Soc. China Eng. Ed.* **2012**, *22*, 1824–1830. [[CrossRef](#)]
12. Yang, Y.; Zhan, L.; Ma, Q.; Feng, J.; Li, X. Effect of pre-deformation on creep age forming of AA2219 plate: Springback, microstructures and mechanical properties. *J. Mater. Process. Technol.* **2016**, *229*, 697–702. [[CrossRef](#)]
13. Lin, Y.C.; Jiang, Y.Q.; Chen, X.M.; Wen, D.X.; Zhou, H.M. Effect of creep-aging on precipitates of 7075 aluminum alloy. *Mater. Sci. Eng. A* **2013**, *588*, 347–356. [[CrossRef](#)]
14. Lin, Y.C.; Zhang, J.-L.; Liu, G.; Liang, Y.-J. Effects of pre-treatments on aging precipitates and corrosion resistance of a creep-aged Al-Zn-Mg-Cu alloy. *Mater. Des.* **2015**, *83*, 866–875. [[CrossRef](#)]
15. Lin, Y.C.; Jiang, Y.-Q.; Zhang, J.-L.; Chen, X.-M. Influence of Stress-Aging Processing on Precipitates and Mechanical Properties of a 7075 Aluminum Alloy. *Adv. Eng. Mater.* **2018**, *20*, 1700583. [[CrossRef](#)]
16. CHEN, J.; CHEN, Z.; GUO, X.; REN, J.; DENG, Y. Microstructure and property of stress aged Al-Cu single crystal under various applied stresses. *Trans. Nonferrous Met. Soc. China* **2016**, *26*, 2838–2845. [[CrossRef](#)]
17. Hunsicker, H.Y. Dimensional changes in heat treating aluminum alloys. *Metall. Trans. A* **1980**, *11*, 759–773. [[CrossRef](#)]
18. Zhu, A.W.; Starke, E.A. Stress aging of Al-xCu alloys: Experiments. *Acta Mater.* **2001**, *49*, 2285–2295. [[CrossRef](#)]
19. Inforzato, D.J.; Costa Junior, P.R.; Fernandez, F.F.; Travessa, D.N. Creep-age forming of AA7475 aluminum panels for aircraft lower wing skin application. *Mater. Res.* **2012**, *15*, 596–602. [[CrossRef](#)]
20. Emani, S.V.; Benedyk, J.; Nash, P.; Chen, D. Double aging and thermomechanical heat treatment of AA7075 aluminum alloy extrusions. *J. Mater. Sci.* **2009**, *44*, 6384–6391. [[CrossRef](#)]
21. Lloyd, D.J.; Chaturvedi, M.C. A calorimetric study of aluminium alloy AA-7075. *J. Mater. Sci.* **1982**, *17*, 1819–1824. [[CrossRef](#)]

22. Godard, D.; Archambault, P.; Aeby-Gautier, E.; Lapasset, G. Precipitation sequences during quenching of the AA 7010 alloy. *Acta Mater.* **2002**, *50*, 2319–2329. [[CrossRef](#)]
23. Scharifi, E.; Savaci, U.; Kavaklioglu, Z.B.; Weidig, U.; Turan, S.; Steinhoff, K. Effect of thermo-mechanical processing on quench-induced precipitates morphology and mechanical properties in high strength AA7075 aluminum alloy. *Mater. Charact.* **2021**, *174*, 111026. [[CrossRef](#)]
24. Zheng, K.; Dong, Y.; Zheng, J.H.; Foster, A.; Lin, J.; Dong, H.; Dean, T.A. The effect of hot form quench (HFQ[®]) conditions on precipitation and mechanical properties of aluminium alloys. *Mater. Sci. Eng. A* **2019**, *761*, 138017. [[CrossRef](#)]
25. Milkereit, B.; Starink, M.J.; Rometsch, P.A.; Schick, C.; Kessler, O. Review of the quench sensitivity of aluminium alloys: Analysis of the kinetics and nature of quench-induced precipitation. *Materials* **2019**, *12*, 4083. [[CrossRef](#)] [[PubMed](#)]
26. Schick, C.; Mathot, V. *Fast Scanning Calorimetry*; Springer International Publishing: Berlin/Heidelberg, Germany, 2016; ISBN 9783319313290.
27. Osten, J.; Milkereit, B.; Schick, C.; Kessler, O. Dissolution and Precipitation Behaviour during Continuous Heating of Al–Mg–Si Alloys in a Wide Range of Heating Rates. *Materials* **2015**, *8*, 2830–2848. [[CrossRef](#)]
28. Liu, M.; Wu, Z.; Yang, R.; Wei, J.; Yu, Y.; Skaret, P.C.; Roven, H.J. DSC analyses of static and dynamic precipitation of an Al–Mg–Si–Cu aluminum alloy. *Prog. Nat. Sci. Mater. Int.* **2015**, *25*, 153–158. [[CrossRef](#)]
29. Liu, M.P.; Jiang, T.H.; Wang, J.; Liu, Q.; Wu, Z.J.; Yu, Y.D.; Skaret, P.C.; Roven, H.J. Aging behavior and mechanical properties of 6013 aluminum alloy processed by severe plastic deformation. *Trans. Nonferrous Met. Soc. China Eng. Ed.* **2014**, *24*, 3858–3865. [[CrossRef](#)]
30. Arabi Jeshvaghani, R.; Shahverdi, H.R.; Hadavi, S.M.M. Investigation of the age hardening and operative deformation mechanism of 7075 aluminum alloy under creep forming. *Mater. Sci. Eng. A* **2012**, *552*, 172–178. [[CrossRef](#)]
31. Osten, J.; Lux, C.; Milkereit, B.; Reich, M. Olaf Kessler Stress Induced Precipitation during Quenching of Aluminium Alloys | Scientific.Net. *Mater. Sci. Forum* **2016**, *877*, 159–165. [[CrossRef](#)]
32. Scharifi, E.; Knoth, R.; Weidig, U. Thermo-mechanical forming procedure of high strength Aluminum sheet with improved mechanical properties and process efficiency. *Procedia Manuf.* **2019**, *29*, 481–489. [[CrossRef](#)]
33. Hebbar, S.; Kertsch, L.; Butz, A. Optimizing heat treatment parameters for the w-temper forming of 7xxx series aluminum alloys. *Metals* **2020**, *10*, 1361. [[CrossRef](#)]
34. Sajadifar, S.V.; Moeini, G.; Scharifi, E.; Lauhoff, C.; Böhm, S.; Niendorf, T. On the Effect of Quenching on Postweld Heat Treatment of Friction-Stir-Welded Aluminum 7075 Alloy. *J. Mater. Eng. Perform.* **2019**, *28*, 5255–5265. [[CrossRef](#)]
35. Polak, S.; Kaczyński, P.; Gronostajski, Z.; Jaskiewicz, K.; Krawczyk, J.; Skwarski, M.; Zwierzchowski, M.; Chorzępa, W. Warm forming of 7075 aluminum alloys. *Procedia Eng. Procedia Manuf.* **2017**, *207*, 2399–2404. [[CrossRef](#)]
36. Lin, J.; Bao, X.; Hou, Y.; Min, J.; Qu, X.; Tao, Z.; Chen, J. Investigation on Yield Behavior of 7075-T6 Aluminum Alloy at Elevated Temperatures. *Chin. J. Mech. Eng. Eng. Ed.* **2020**, *33*, 76. [[CrossRef](#)]
37. Fröck, H.; Reich, M.; Milkereit, B.; Kessler, O. Scanning Rate Extension of Conventional DSCs through Indirect Measurements. *Materials* **2019**, *12*, 1085. [[CrossRef](#)] [[PubMed](#)]
38. Luo, J.; Luo, H.; Li, S.; Wang, R.; Ma, Y. Effect of pre-ageing treatment on second nucleating of GPII zones and precipitation kinetics in an ultrafine grained 7075 aluminum alloy. *Mater. Des.* **2020**, *187*, 108402. [[CrossRef](#)]
39. Hargarter, H.; Lyttle, M.T.; Starke, E.A. Effects of preferentially aligned precipitates on plastic anisotropy in Al–Cu–Mg–Ag and Al–Cu alloys. *Mater. Sci. Eng. A* **1998**, *257*, 87–99. [[CrossRef](#)]
40. Jiang, M.G.; Xu, C.; Yan, H.; Nakata, T.; Chen, Z.W.; Lao, C.S.; Chen, R.S.; Kamado, S.; Han, E.H. Quasi-in-situ observing the rare earth texture evolution in an extruded Mg–Zn–Gd alloy with bimodal microstructure. *J. Magnes. Alloy.* **2020**. [[CrossRef](#)]
41. Sakai, T.; Belyakov, A.; Kaibyshev, R.; Miura, H.; Jonas, J.J. Dynamic and post-dynamic recrystallization under hot, cold and severe plastic deformation conditions. *Prog. Mater. Sci.* **2014**, *60*, 130–207. [[CrossRef](#)]
42. Shao, Z.; Jiang, J.; Lin, J. Feasibility study on direct flame impingement heating applied for the solution heat treatment, forming and cold die quenching technique. *J. Manuf. Process.* **2018**, *36*, 398–404. [[CrossRef](#)]
43. Harrison, N.R.; Luckey, S.G. Hot Stamping of a B-Pillar Outer from High Strength Aluminum Sheet AA7075. *SAE Int. J. Mater. Manuf.* **2014**, *7*, 2014–01–0981. [[CrossRef](#)]
44. Panigrahi, S.K.; Jayaganthan, R. Effect of annealing on thermal stability, precipitate evolution, and mechanical properties of cryorolled Al 7075 alloy. *Metall. Mater. Trans. A Phys. Metall. Mater. Sci.* **2011**, *42*, 3208–3217. [[CrossRef](#)]
45. Huang, K.; Logé, R.E. Zener Pinning. In *Reference Module in Materials Science and Materials Engineering*; Elsevier: Amsterdam, The Netherlands, 2016.
46. Liang, P.C.; Lin, K.L. Non-deformation recrystallization of metal with electric current stressing. *J. Alloys Compd.* **2017**, *722*, 690–697. [[CrossRef](#)]
47. Alaneme, K.K.; Okotete, E.A. Recrystallization mechanisms and microstructure development in emerging metallic materials: A review. *J. Sci. Adv. Mater. Devices* **2019**, *4*, 19–33. [[CrossRef](#)]
48. Humphreys, F.J.; Hatherly, M. *Recrystallization and Related Annealing Phenomena*; Elsevier: Amsterdam, The Netherlands, 2004; ISBN 9780080441641.
49. Gleiter, H. The mechanism of grain boundary migration. *Acta Metall.* **1969**, *17*, 565–573. [[CrossRef](#)]
50. Starke, E.A. Aluminum Alloys: Thermomechanical Processing. In *Encyclopedia of Materials: Science and Technology*; Elsevier: Amsterdam, The Netherlands, 2001; pp. 118–121.

51. Gronsky, R.; Furrer, P. Grain Boundary Precipitation in Aluminum Alloys: Effect of Boundary Structure. *Metall. Trans. A Phys. Metall. Mater. Sci.* **1981**, *12A*, 121–127. [[CrossRef](#)]
52. De Hass, M.; De Hosson, J.T.M. Grain boundary segregation and precipitation in aluminum alloys. *Scr. Mater.* **2001**, *44*, 281–286. [[CrossRef](#)]
53. Ardell, A.J. On the coarsening of grain boundary precipitates. *Acta Metall.* **1972**, *20*, 601–609. [[CrossRef](#)]
54. Kumar, P.V.; Reddy, G.M.; Rao, K.S. Microstructure, mechanical and corrosion behavior of high strength AA7075 aluminium alloy friction stir welds—Effect of post weld heat treatment. *Def. Technol.* **2015**, *11*, 362–369. [[CrossRef](#)]
55. Mahoney, M.W.; Rhodes, C.G.; Flintoff, J.G.; Bingel, W.H.; Spurling, R.A. Properties of friction-stir-welded 7075 T651 aluminum. *Metall. Mater. Trans. A* **1998**, *29*, 1955–1964. [[CrossRef](#)]
56. Rhodes, C.G.; Mahoney, M.W.; Bingel, W.H.; Spurling, R.A.; Bampton, C.C. Effects of friction stir welding on microstructure of 7075 aluminum. *Scr. Mater.* **1997**, *36*, 69–75. [[CrossRef](#)]
57. Jiao, H.; Chen, K.; Chen, S.; Yang, Z.; Xie, P.; Chen, S. Effect of Cu on the Fracture and Exfoliation Corrosion Behavior of Al-Zn-Mg-xCu Alloy. *Metals* **2018**, *8*, 1048. [[CrossRef](#)]
58. Ben Ali, N.; Estevez, R.; Tanguy, D. Heterogeneity of grain boundaries in 5xxx and 7xxx aluminum alloys and its influence on intergranular toughness. *Eng. Fract. Mech.* **2013**, *97*, 1–11. [[CrossRef](#)]
59. Jiang, X.J.; Noble, B.; Holme, B.; Waterloo, G.; Taftø, J. Differential scanning calorimetry and electron diffraction investigation on low-temperature aging in Al-Zn-Mg alloys. *Metall. Mater. Trans. A Phys. Metall. Mater. Sci.* **2000**, *31*, 339–348. [[CrossRef](#)]
60. Park, J.K.; Ardell, A.J. Correlation between microstructure and calorimetric behavior of aluminum alloy 7075 and AlZnMg alloys in various tempers. *Mater. Sci. Eng. A* **1989**, *114*, 197–203. [[CrossRef](#)]
61. Campana, F.; Pilone, D. Effect of heat treatments on the mechanical behaviour of aluminium alloy foams. *Scr. Mater.* **2009**, *60*, 679–682. [[CrossRef](#)]
62. Zhan, L.; Lin, J.; Dean, T.A. A review of the development of creep age forming: Experimentation, modelling and applications. *Int. J. Mach. Tools Manuf.* **2011**, *51*, 1–17. [[CrossRef](#)]
63. Murken, J.; Höhner, R.; Skrotzki, B. Strain path dependence of the precipitate size evolution of an Al-Mg-Li alloy under combined thermal and mechanical loading. *Mater. Sci. Eng. A* **2003**, *363*, 159–170. [[CrossRef](#)]
64. Häusler, I.; Kamachali, R.; Hetaba, W.; Skrotzki, B. Thickening of T1 Precipitates during Aging of a High Purity Al-4Cu-1Li-0.25Mn Alloy. *Materials* **2018**, *12*, 30. [[CrossRef](#)]
65. Zhang, J.; Deng, Y.; Zhang, X. Constitutive modeling for creep age forming of heat-treatable strengthening aluminum alloys containing plate or rod shaped precipitates. *Mater. Sci. Eng. A* **2013**, *563*, 8–15. [[CrossRef](#)]
66. Guo, W.; Yang, M.; Zheng, Y.; Zhang, X.; Li, H.; Wen, X.; Zhang, J. Influence of elastic tensile stress on aging process in an Al-Zn-Mg-Cu alloy. *Mater. Lett.* **2013**, *106*, 14–17. [[CrossRef](#)]
67. Skrotzki, B.; Shiflet, G.J.; Starke, E.A. On the effect of stress on nucleation and growth of precipitates in an Al-Cu-Mg-Ag alloy. *Metall. Mater. Trans. A Phys. Metall. Mater. Sci.* **1996**, *27*, 3431–3444. [[CrossRef](#)]
68. Skrotzki, B.; Murken, J. On the Effect of Stress on Nucleation, Growth, and Coarsening of Precipitates in Age-Hardenable Aluminum Alloys. In *Lightweight Alloys for Aerospace Application*; John Wiley & Sons, Inc.: Hoboken, NJ, USA, 2013; pp. 51–61.